Silicon
https://doi.org/10.1007/s12633-024-02915-y

RESEARCH

Investigation of ORR and OER Mechanisms by Co- and Fe-doped Silicon Nanocages (Si_{48} and Si_{60}) and Co- and Fe-doped Silicon Nanotubes (SiNT(5, 0) and SiNT(6, 0)) as Acceptable Catalysts

Diana Katherine Campoverde Santos[1] · Mohammed Ahmed Mustafa[2] · Pooja Bansal[3,4] · Harpreet Kaur[5,6] · Mahamedha Deorari[7] · Farag M. A. Altalbawy[8,9] · Dheyaa Yahaia Alhameedi[10] · Mahmood Hasen shuhata Alubiady[11] · Ahmed Muzahem Al-Ani[12] · Sally Salih Jumaa[13] · Munther Kadhim Abosaoda[14,15,16] · Li Zhang[17]

Received: 29 October 2023 / Accepted: 13 February 2024

Abstract

In this work, the catalytic activity of Co-Si_{48}, Co-Si_{60}, Co-SiNT (5, 0), Co-SiNT (6, 0), Fe-Si_{48}, Fe-Si_{60}, Fe-SiNT (5, 0), Fe-SiNT (6, 0) as catalysts of oxygen reduction reaction (ORR) and oxygen evolution reaction (OER) are examined. The Fe doped Si-nanotubes and Si-nanocages have more negative the formation energy and adoption energy values than Co doped Si-nanotubes and Si-nanocages. Results indicated that the reactions step of OOH* creation for OER and OH* elimination for ORR are the potential-determining steps. The *O has the most negative adsorption energy than *OH, *OOH, *H, O_2 and H_2O species. The H_2O is desorbed on Si-nanostructures with low adsorption energy. The Gibbs free energy values of reaction step 1 and step 2 ($OH^- + \text{Si-nanostructure} \rightarrow \text{Si-nanostructure-*OH} + e^- \rightarrow \text{Si-nanostructure -*O} + H_2O + e^-$) on Co and Fe doped Si-nanostructures are negative values. The overpotential of ORR processes on Co-Si_{48}, Co-Si_{60}, Co-SiNT (5, 0), Co-SiNT (6, 0), Fe-Si_{48}, Fe-Si_{60}, Fe-SiNT (5, 0), Fe-SiNT (6, 0) in water are 1.24, 1.20, 1.15, 1.11, 1.07, 1.04, 1.00 and 0.97 eV. The metal doped Si-nanotubes and Si-nanocages have acceptable potential to catalyze the OER and ORR reactions.

Keywords Electrochemistry · Silicon · Nanostructures · Gibbs free energy · Overpotential · OER mechanism · ORR processes

✉ Li Zhang
lizhang1203@chmail.ir

[1] Facultad de Ciencias Pecuarias, Escuela Superior Politécnica de Chimborazo (ESPOCH), Panamericana Sur Km. 1 1/2, Riobamba 060155, Ecuador

[2] Department of Medical Laboratory Technology, University of Imam Jaafar AL-Sadiq, Baghdad, Iraq

[3] Department of Biotechnology and Genetics, Jain (Deemed-to-Be) University, Bengaluru, Karnataka 560069, India

[4] Department of Allied Healthcare and Sciences, Vivekananda Global University, Jaipur, Rajasthan 303012, India

[5] School of Basic & Applied Sciences, Shobhit University, Gangoh, Uttar Pradesh 247341, India

[6] Department of Health & Allied Sciences, Arka Jain University, Jamshedpur, Jharkhand 831001, India

[7] Uttaranchal Institute of Pharmaceutical Sciences, Uttaranchal University, Dehradun, India

[8] Department of Chemistry, University College of Duba, University of Tabuk, Tabuk, Saudi Arabia

[9] National Institute of Laser Enhanced Sciences (NILES), University of Cairo, Giza 12613, Egypt

[10] Department of Anesthesia, College of Health & Medical Technology, Sawa University, Samawah, Almuthana, Iraq

[11] Department of Medical Engineering, Al-Hadi University College, Baghdad 10011, Iraq

[12] Department of Medical Engineering, Al-Nisour University College, Baghdad, Iraq

[13] Department of Medical Engineering, National University of Science and Technology, Nasiriyah, Dhi Qar, Iraq

[14] College of Pharmacy, the Islamic University, Najaf, Iraq

[15] College of Pharmacy, the Islamic University of Al Diwaniyah, Al Diwaniyah, Iraq

[16] College of Pharmacy, the Islamic University of Babylon, Al Diwaniyah, Iraq

[17] School of Mechanical and Electrical Engineering, Guangzhou Railway Polytechnic, Guangzhou 511370, China

Published online: 23 February 2024

1 Introduction

In recent years, the new nano-catalysts have been selected for oxygen reduction reaction (ORR) and oxygen evolution reaction (OER) processes in electrochemistry [1–3]. The metal based catalysts have low stability and selectivity to catalyze the ORR and OER processes [4–6]. The metal doped nanostructures such as nanotubes and nanocages have been proposed as acceptable catalysts for reactions in electrochemistry [7–10].

Researchers have been demonstrated that the silicon nanocages and silicon nanotubes can be utilized for ORR and OER processes based on their high surface and high selectivity and high stability [11–13]. Researchers have indicated that the various metal atoms such as Co and Fe can be doped on silicon nanocages and silicon nanotubes and these metals are active sites and potential positions of these catalysts to adsorb the important gas molecules [14–16].

Yu and et al. [17, 18] have used the theoretical models to calculated the effects of point defects on catalytic activity of silicene and their applications in the Li–O batteries. They have examined the nucleation mechanisms and decomposition reactions of Li_4O_2 processes on Tl_2O in Li – O batteries by theoretical models. They have confirmed that the adsorbed LiO on Tl2 O cannot change the conductance in ORR and OER processes [17, 18]. They have indicated that the silicenes can catalyze the ORR and OER with high efficiency in normal temperature. They have demonstrated that the silicenes have high performance to use in batteries to obtain the ORR intermediates in normal temperature [17, 18].

Li and et al. [19–21] have examined the activity of NbO, MoO_3, MnO_2 and Nb_2O_5 compounds in reactions of metal batteries and their catalytic activity for OER and ORR. They have proposed the new strategies by oxygen deficiency to improve and increase the catalyst efficiency of OER and ORR processes. they have indicated that the MoO3 have important effects to prevent the oxygen production in Li–O batteries and Na–O batteries. They have confirmed that the MoO3 can do the reduction of metal peroxides as effective strategy to avoid the un-normal reactions [19–21].

The potential of Co and Fe doped Si-nanotubes (Co-SiNT (5, 0), Co-SiNT (6, 0), Fe-SiNT (5, 0) and Fe-SiNT (6, 0)) and Co and Fe doped Si-nanocages (Co-Si_{48}, Co-Si_{60}, Fe-Si_{48} and Fe-Si_{60}) to catalyze the OER and ORR are studied. The effects of water as solvent on absorption of species of ORR and OER on metal doped Si-nanotubes and Si-nanocages and on catalytic activity of Co and Fe doped Si-nanotubes and Si-nanocages to catalyze the ORR and OER processes are examined in normal temperature [22–24].

The formation energy ($E_{formation}$) and adoption energy ($E_{adoption}$) of Co-Si_{48}, Co-Si_{60}, Co-SiNT (5, 0), Co-SiNT (6, 0), Fe-Si_{48}, Fe-Si_{60}, Fe-SiNT (5, 0), Fe-SiNT (6, 0) are calculated and compared [25–27]. The adsorption energy ($\Delta E_{adsorption}$) of Co-Si_{48}, Co-Si_{60}, Co-SiNT (5, 0), Co-SiNT (6, 0), Fe-Si_{48}, Fe-Si_{60}, Fe-SiNT (5, 0), Fe-SiNT (6, 0) to adsorb the ORR and OER species (O*, *OH, *OOH, *H, H_2O and O_2) are calculated and compared in gas phase and water [28–30].

The orbital energy and charge (q) values of Co-Si_{48}, Co-Si_{60}, Co-SiNT (5, 0), Co-SiNT (6, 0), Fe-Si_{48}, Fe-Si_{60}, Fe-SiNT (5, 0), Fe-SiNT (6, 0) are investigated [31]. The orbital energy and charge (q) values of complexes of metal doped Si nanocages and Co and Fe doped Si nanotubes with ORR and OER species including the O*, *OH, *OOH, *H and O_2 are calculated [32].

The $\Delta G_{reaction}$ of OER and ORR reaction steps ($OH^- + Si\text{-}nanostructure \rightarrow Si\text{-}nanostructure\text{-}*OH + e^- \rightarrow Si\text{-}nanostructure\ \text{-}*O + H_2O + e^- \rightarrow Si\text{-}nanostructure\ \text{-}*OOH + e^- \rightarrow surface* + O_2 + H_2O + e^-$) on surfaces of Co-$Si_{48}$, Co-$Si_{60}$, Co-SiNT (5, 0), Co-SiNT (6, 0), Fe-Si_{48}, Fe-Si_{60}, Fe-SiNT (5, 0), Fe-SiNT (6, 0) in gas phase and water are investigated [33]. The overpotential of ORR and OER on Co-Si_{48}, Co-Si_{60}, Co-SiNT (5, 0), Co-SiNT (6, 0), Fe-Si_{48}, Fe-Si_{60}, Fe-SiNT (5, 0), Fe-SiNT (6, 0) are examined [34].

2 Computational Details

The structures of Co and Fe doped Si nanocages and Co and Fe doped Si nanotubes (Co-Si_{48}, Co-Si_{60}, Co-SiNT (5, 0), Co-SiNT (6, 0), Fe-Si_{48}, Fe-Si_{60}, Fe-SiNT (5, 0), Fe-SiNT (6, 0)) are optimized by M06-2X functional and cc-pVQZ basis set in GAMESS software [35–37]. The structures of complexes of Co-Si_{48}, Co-Si_{60}, Co-SiNT (5, 0), Co-SiNT (6, 0), Fe-Si_{48}, Fe-Si_{60}, Fe-SiNT (5, 0), Fe-SiNT (6, 0) with ORR and OER processes are optimized by M06-2X functional and cc-pVQZ basis set [38]. The frequencies of optimized structures of Co-Si_{48}, Co-Si_{60}, Co-SiNT (5, 0), Co-SiNT (6, 0), Fe-Si_{48}, Fe-Si_{60}, Fe-SiNT (5, 0), Fe-SiNT (6, 0) and there are examined by M06-2X functional and cc-pVQZ basis set [39–41].

The ability of Co-Si_{48}, Co-Si_{60}, Co-SiNT (5, 0), Co-SiNT (6, 0), Fe-Si_{48}, Fe-Si_{60}, Fe-SiNT (5, 0), Fe-SiNT (6, 0) to adsorb the species are invesigated by $\Delta E_{adsorption}$ via Eqs. 1 and 2 as following [42]:

$$\Delta E_{adsorption} = E_{Si-nanotube-molecule} - E_{Si-nanotube} - E_{molecule} \quad (1)$$

$$\Delta E_{adsorption} = E_{Si-nanocage-molecule} - E_{Si-nanocage} - E_{molecule} \quad (2)$$

The $E_{Si\text{-}nanotube}$ and $E_{Si\text{-}nanocage}$ are total energy of Co and Fe doped Si-nanotubes (Co-SiNT (5, 0), Co-SiNT (6, 0),

Fe-SiNT (5, 0) and Fe-SiNT (6, 0)) and Co and Fe doped Si-nanocages (Co-Si_{48}, Co-Si_{60}, Fe-Si_{48} and Fe-Si_{60}), respectively. The $E_{molecule}$ are total energy of important species of ORR and OER processes including the O*, *OH, *OOH, *H, H_2O and O_2. The $E_{Si\text{-}nanotube\text{-}molecule}$ and $E_{Si\text{-}nanocage\text{-}molecule}$ are total energy of complexes of Co and Fe doped Si-nanotubes (Co-SiNT (5, 0), Co-SiNT (6, 0), Fe-SiNT (5, 0) and Fe-SiNT (6, 0)) and Co and Fe doped Si-nanocages (Co-Si_{48}, Co-Si_{60}, Fe-Si_{48} and Fe-Si_{60}) with species including the O*, *OH, *OOH, *H and O_2, respectively.

The main reaction for OER and ORR processes on Co-Si_{48}, Co-Si_{60}, Co-SiNT (5, 0), Co-SiNT (6, 0), Fe-Si_{48}, Fe-Si_{60}, Fe-SiNT (5, 0), Fe-SiNT (6, 0) is presented in Eq. 3 and the $\Delta G_{reaction}$ of OER and ORR processes are calculated by Eq. 4 as following [43]:

$$4OH^- \rightarrow O_2 + 2H_2O + 4e^- \tag{3}$$

$$\Delta G_{reaction} = \Delta G_{adsorption} + \Delta G_U + \Delta G_{pH} \tag{4}$$

The $\Delta G_{reaction}$ is free Gibbs energy of complexes of Co and Fe doped Si-nanotubes and Co and Fe doped Si-nanocages with species and the ΔG_U is defined by $-neU$, the U is electrode potential and ΔG_{pH} is free energy correction [44–46].

The effects of water as solvent on absorption of species on Co and Fe doped Si-nanotubes and Si-nanocages and on catalytic activity of Co and Fe doped Si-nanotubes and Si-nanocages to catalyze the ORR and OER processes are examined by COSMO ((COnductor-like Screening MOdel)) model [47–50].

The orbital energy and charge (q) values of Co and Fe doped Si nanocages and Co and Fe doped Si nanotubes (Co-Si_{48}, Co-Si_{60}, Co-SiNT (5, 0), Co-SiNT (6, 0), Fe-Si_{48}, Fe-Si_{60}, Fe-SiNT (5, 0), Fe-SiNT (6, 0)) and their complexes including the O*, *OH, *OOH, *H and O_2 are calculated by M06-2X functional and cc-pVQZ basis set [51–53].

3 Results and Discussion

3.1 Co and Fe Doped Si-nanostructures

The structures of Co-Si_{48}, Co-Si_{60}, Co-SiNT (5, 0), Co-SiNT (6, 0), Fe-Si_{48}, Fe-Si_{60}, Fe-SiNT (5, 0), Fe-SiNT (6, 0) are presented in Fig. 1. The important bond lengths of Co-Si_{48}, Co-Si_{60}, Co-SiNT (5, 0), Co-SiNT (6, 0), Fe-Si_{48}, Fe-Si_{60}, Fe-SiNT (5, 0), Fe-SiNT (6, 0) are reported in Fig. 1. The formation energy ($E_{formation}$) of Co-Si_{48}, Co-Si_{60}, Co-SiNT (5, 0), Co-SiNT (6, 0), Fe-Si_{48}, Fe-Si_{60}, Fe-SiNT (5, 0), Fe-SiNT (6, 0) are calculated by Eqs. 5 and 6 [54–56]:

$$E_{formation} = E_{Si-nanotube} - n * E_{Si} - E_{Metal} \tag{5}$$

$$E_{formation} = E_{Si-nanocage} - m * E_{Si} - E_{Metal} \tag{6}$$

The $E_{Si\text{-}nanotube}$ and $E_{Si\text{-}nanocage}$ are total energy of Co and Fe doped Si-nanotubes (Co-SiNT (5, 0), Co-SiNT (6, 0), Fe-SiNT (5, 0) and Fe-SiNT (6, 0)) and Co and Fe doped Si-nanocages (Co-Si_{48}, Co-Si_{60}, Fe-Si_{48} and Fe-Si_{60}), respectively. The E_{Metal} is total energy of an Fe and Co atoms in their bulk crystal. The *n* is the number of silicon atoms in Co and Fe doped Si-nanocages (Co-Si_{48}, Co-Si_{60}, Fe-Si_{48} and Fe-Si_{60}) and the *m* is the number of silicon atoms in Co and Fe doped Si-nanotubes (Co-SiNT (5, 0), Co-SiNT (6, 0), Fe-SiNT (5, 0) and Fe-SiNT (6, 0)).

The formation energy ($E_{formation}$) of Co-Si_{48}, Co-Si_{60}, Co-SiNT (5, 0), Co-SiNT (6, 0), Fe-Si_{48}, Fe-Si_{60}, Fe-SiNT (5, 0), Fe-SiNT (6, 0) are reported in Table 1. In gas phase, the $E_{formation}$ of Co-SiNT (5, 0), Co-SiNT (6, 0), Fe-SiNT (5, 0) and Fe-SiNT (6, 0) are -4.35, -4.45, -4.79 and -4.90 eV, respectively. In gas phase, the $E_{formation}$ of Co-Si_{48}, Co-Si_{60}, Fe-Si_{48} and Fe-Si_{60} are -4.15, -4.25, -4.56 and -4.67 eV, respectively. In water, the $E_{formation}$ of Co-SiNT (5, 0), Co-SiNT (6, 0), Fe-SiNT (5, 0) and Fe-SiNT (6, 0) are -5.37, -5.50, -5.91 and -6.05 eV. The $E_{formation}$ of Co-Si_{48}, Co-Si_{60}, Fe-Si_{48} and Fe-Si_{60} are -5.11, -5.24, -5.63 and -5.77 eV, respectively.

The adoption energy ($E_{adoption}$) of Co-Si_{48}, Co-Si_{60}, Co-SiNT (5, 0), Co-SiNT (6, 0), Fe-Si_{48}, Fe-Si_{60}, Fe-SiNT (5, 0), Fe-SiNT (6, 0) are calculated by Eqs. 7 and 8 [57–59]:

$$E_{adoption} = E_{Metal-Si-nanotube} - E_{Si-nanocage} - E_{Metal} \tag{7}$$

$$E_{adoption} = E_{Metal-Si-nanocage} - E_{Si-nanocage} - E_{Metal} \tag{8}$$

The E_{Metal} is total energy of an Fe and Co atoms in their bulk crystal. The $E_{Metal\text{-}Si\text{-}nanotube}$ and $E_{Metal\text{-}Si\text{-}nanocage}$ are total energy of Co-Si_{48}, Co-Si_{60}, Co-SiNT (5, 0), Co-SiNT (6, 0), Fe-Si_{48}, Fe-Si_{60}, Fe-SiNT (5, 0), Fe-SiNT (6, 0), respectively. The $E_{Si\text{-}nanotube}$ and $E_{Si\text{-}nanocage}$ are total energy of Si-nanotubes (SiNT (5, 0), SiNT (6, 0), SiNT (5, 0) and SiNT (6, 0)) and Si-nanocages (Si_{48}, Si_{60}, Si_{48} and Si_{60}), respectively.

The adoption energy ($E_{adoption}$) of Co-Si_{48}, Co-Si_{60}, Co-SiNT (5, 0), Co-SiNT (6, 0), Fe-Si_{48}, Fe-Si_{60}, Fe-SiNT (5, 0), Fe-SiNT (6, 0) are reported in Table 1. In gas phase, the $E_{adoption}$ of Co-SiNT (5, 0), Co-SiNT (6, 0), Fe-SiNT (5, 0) and Fe-SiNT (6, 0) are -3.13, -3.27, -3.71 and -3.87 eV, respectively. In gas phase, the $E_{adoption}$ of Co-Si_{48}, Co-Si_{60}, Fe-Si_{48} and Fe-Si_{60} are -2.88, -3.00, -3.41 and -3.56 eV, respectively. In water, the $E_{adoption}$ of Co-SiNT (5, 0), Co-SiNT (6, 0), Fe-SiNT (5, 0) and Fe-SiNT (6, 0) are -3.86, -4.03, -4.58 and -4.78 eV, respectively. In water, the $E_{adoption}$ of Co-Si_{48}, Co-Si_{60}, Fe-Si_{48} and Fe-Si_{60} are -3.55, -3.70, -4.21 and -4.39 eV, respectively.

The $E_{adoption}$ and $E_{formation}$ values of Co-Si_{48}, Co-Si_{60}, Co-SiNT (5, 0), Co-SiNT (6, 0), Fe-Si_{48}, Fe-Si_{60}, Fe-SiNT (5, 0), Fe-SiNT (6, 0) are negative values and these metal

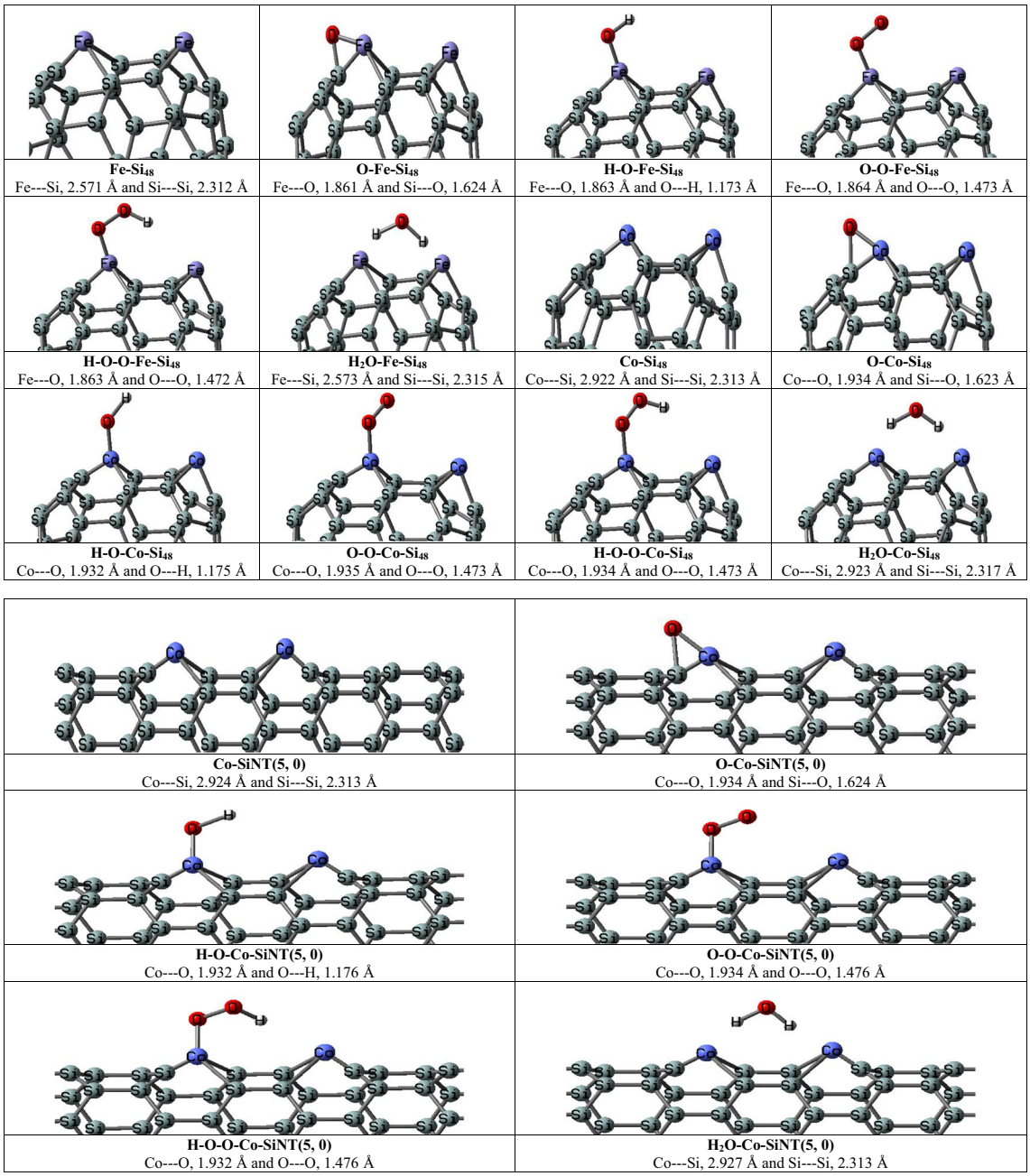

Fig. 1 The structures of metal doped Si-nanostructures and their complexes of ORR and OER species and their important bond lengths

doped Si-nanotubes and Si-nanocages are stable from thermodynamic view point. The $E_{adoption}$ and $E_{formation}$ values of Co-Si_{48}, Co-Si_{60}, Co-SiNT (5, 0), Co-SiNT (6, 0), Fe-Si_{48}, Fe-Si_{60}, Fe-SiNT (5, 0), Fe-SiNT (6, 0) are negative values and these metal doped Si-nanotubes and Si-nanocages are stable from thermodynamic view point.

The calculated orbital energy of HOMO (E_{HOMO}), LUMO (E_{LUMO}) and HOMO–LUMO gap ($E_{HLG} = E_{HOMO} - E_{LUMO}$) and charge (q) values of Co-Si_{48}, Co-Si_{60}, Co-SiNT (5, 0), Co-SiNT (6, 0), Fe-Si_{48}, Fe-Si_{60}, Fe-SiNT (5, 0), Fe-SiNT (6, 0) are presented in Table 2. The E_{HLG} values of Co-Si_{48}, Co-Si_{60}, Co-SiNT (5, 0), Co-SiNT (6, 0), Fe-Si_{48}, Fe-Si_{60}, Fe-SiNT (5, 0), Fe-SiNT (6, 0) are 2.04, 1.86, 1.68, 1.49, 1.31, 1.13, 0.93 and 0.67 eV, respectively. The q values of Co-Si_{48}, Co-Si_{60}, Co-SiNT (5, 0), Co-SiNT (6, 0), Fe-Si_{48}, Fe-Si_{60}, Fe-SiNT (5, 0), Fe-SiNT (6, 0) are 0.912, 0.925, 0.938, 0.952, 0.966, 0.978, 0.990 and 0.998 *e*, respectively. The Fe doped Si-nanotubes and Si-nanocages have lower E_{HLG} values and higher q values than Co doped Si-nanotubes and Si-nanocages. The metal doped Si-nanotubes have

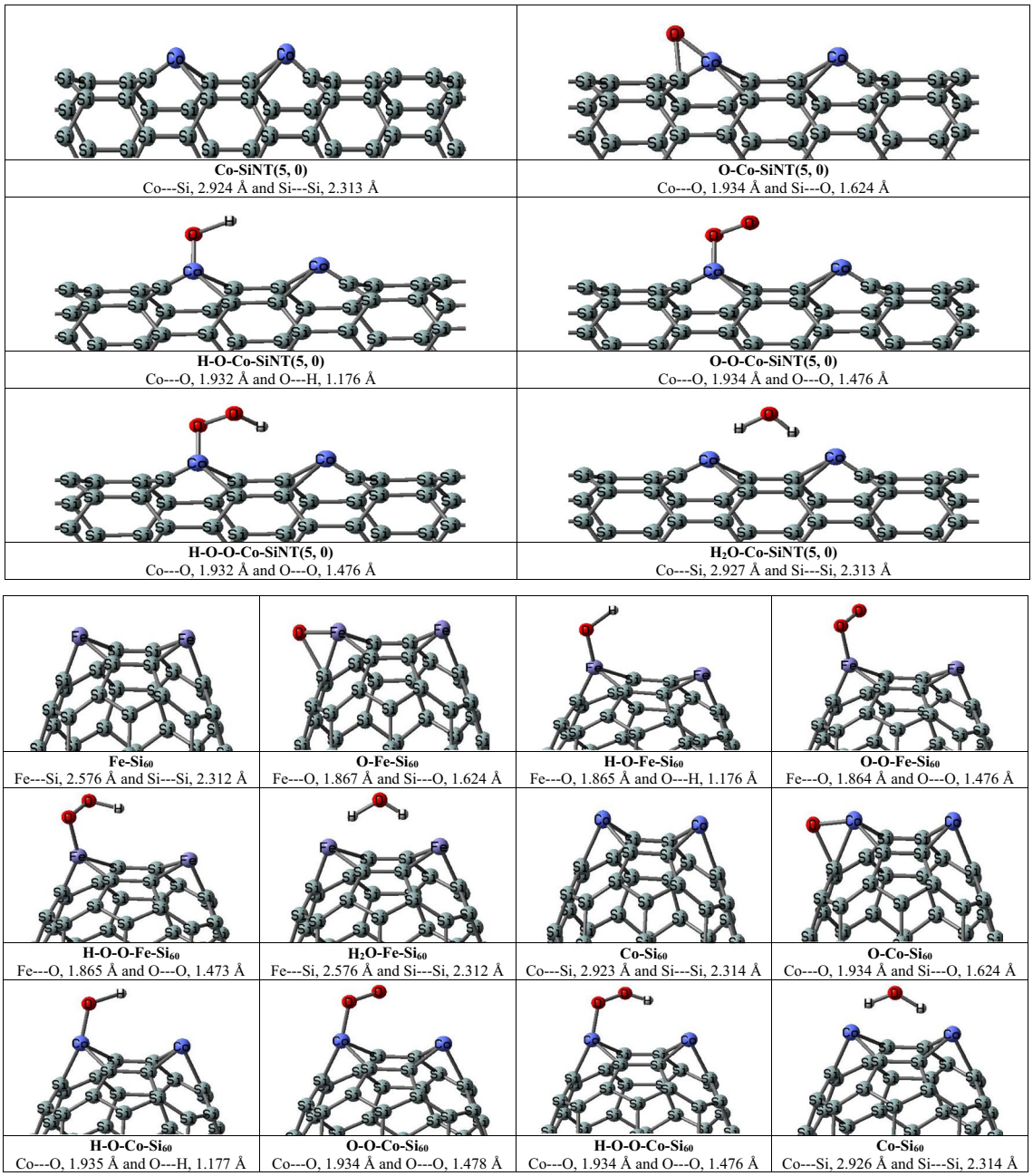

Fig. 1 (continued)

lower E_{HLG} values and higher q values than Co and Fe doped Si-nanocages.

3.2 Adsorption of ORR and OER Species on Metal Doped Si-Nanostructures

The potential of Co-Si_{48}, Co-Si_{60}, Co-SiNT (5, 0), Co-SiNT (6, 0), Fe-Si_{48}, Fe-Si_{60}, Fe-SiNT (5, 0), Fe-SiNT (6, 0) to adsorb the ORR and OER species (O*, *OH, *OOH, *H, H_2O and O_2) are calculated by $\Delta E_{adsorption}$ via Eqs. 1 and 2. The $\Delta E_{adsorption}$ of ORR and OER species (O*, *OH, *OOH, *H, H_2O and O_2) on Co-Si_{48}, Co-Si_{60}, Co-SiNT (5, 0), Co-SiNT (6, 0), Fe-Si_{48}, Fe-Si_{60}, Fe-SiNT (5, 0), Fe-SiNT (6, 0) are reported in Table 1. The structures of complexes of Co-Si_{48}, Co-Si_{60}, Co-SiNT (5, 0), Co-SiNT (6, 0), Fe-Si_{48}, Fe-Si_{60}, Fe-SiNT (5, 0), Fe-SiNT (6, 0) with species are presented in Fig. 2. The important bond lengths of complexes of Fe- and Co-doped Si-nanostructures with OER and ORR species are reported in Fig. 2.

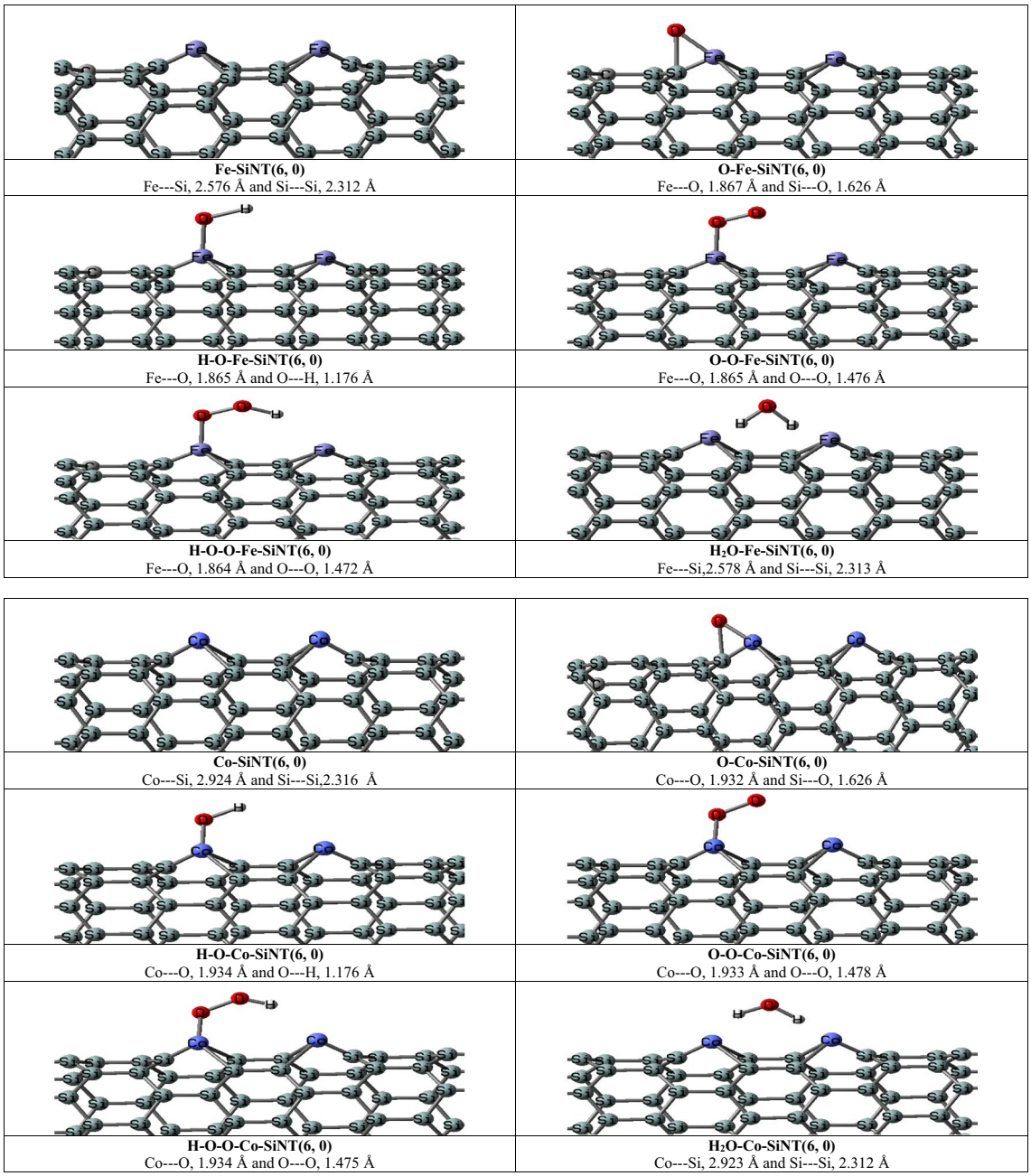

Fig. 1 (continued)

In gas phase, the $\Delta E_{adsorption}$ of *OH on Co-Si_{48}, Co-Si_{60}, Co-SiNT (5, 0) and Co-SiNT (6, 0) are -3.26, -3.48, -3.71 and -3.96 eV, respectively. The $\Delta E_{adsorption}$ of *OH on Fe-Si_{48}, Fe-Si_{60}, Fe-SiNT (5, 0), Fe-SiNT (6, 0) in water are -4.21, -4.51, -4.81 and -5.13 eV, respectively. In gas phase, the $\Delta E_{adsorption}$ of O_2 on Co-Si_{48}, Co-Si_{60}, Co-SiNT (5, 0) and Co-SiNT (6, 0) are -0.45, -0.48, -0.51 and -0.55 eV, respectively. The $\Delta E_{adsorption}$ of O_2 on Fe-Si_{48}, Fe-Si_{60}, Fe-SiNT (5, 0), Fe-SiNT (6, 0) in water are -0.72, -0.77, -0.82 and -0.87 eV, respectively.

In gas phase, the $\Delta E_{adsorption}$ of *O on Co-Si_{48}, Co-Si_{60}, Co-SiNT (5, 0) and Co-SiNT (6, 0) are -3.54, -3.78, -4.03 and -4.30 eV, respectively. The $\Delta E_{adsorption}$ of *O on Fe-Si_{48}, Fe-Si_{60}, Fe-SiNT (5, 0), Fe-SiNT (6, 0) in water are -5.66, -6.04, -6.45 and -6.68 eV, respectively. In gas phase, the $\Delta E_{adsorption}$ of *OOH on Co-Si_{48}, Co-Si_{60}, Co-SiNT (5, 0) and Co-SiNT (6, 0) are -1.73, -1.84, -1.97 and -2.10 eV, respectively. The $\Delta E_{adsorption}$ of *OOH on Fe-Si_{48}, Fe-Si_{60}, Fe-SiNT (5, 0), Fe-SiNT (6, 0) in water are -2.76, -2.95, -3.14 and -3.35 eV, respectively.

Table 1 The $E_{formation}$ in eV and $E_{adoption}$ in eV of metal doped Si-nanostructures in gas phase and water, the $\Delta E_{adsorption}$ in eV of species on metal doped Si-nanostructures at T = 298 K in gas phase and water

Catalysts	$E_{formation}$ in gas phase	$E_{adoption}$ in gas phase	Catalysts	$E_{formation}$ in water	$E_{adoption}$ in water
Co-Si_{48}	-4.15	-2.88	Co-Si_{48}	-5.11	-3.55
Co-Si_{60}	-4.25	-3.00	Co-Si_{60}	-5.24	-3.70
Co-SiNT(5, 0)	-4.35	-3.13	Co-SiNT(5, 0)	-5.37	-3.86
Co-SiNT(6, 0)	-4.45	-3.27	Co-SiNT(6, 0)	-5.50	-4.03
Fe-Si_{48}	-4.56	-3.41	Fe-Si_{48}	-5.63	-4.21
Fe-Si_{60}	-4.67	-3.56	Fe-Si_{60}	-5.77	-4.39
Fe-SiNT(5, 0)	-4.79	-3.71	Fe-SiNT(5, 0)	-5.91	-4.58
Fe-SiNT(6, 0)	-4.90	-3.87	Fe-SiNT(6, 0)	-6.05	-4.78

$\Delta E_{adsorption}$ in gas phase

Catalysts	Co-Si_{48}	Co-Si_{60}	Co-SiNT (5, 0)	Co-SiNT (6, 0)	Fe-Si_{48}	Fe-Si_{60}	Fe-SiNT (5, 0)	Fe-SiNT (6, 0)
Catalyst-*OH	-3.26	-3.48	-3.71	-3.96	-4.22	-4.51	-4.81	-5.13
Catalyst-*O	-3.54	-3.78	-4.03	-4.30	-4.59	-4.90	-5.22	-5.57
Catalyst-*OOH	-1.73	-1.84	-1.97	-2.10	-2.24	-2.39	-2.55	-2.72
Catalyst-O_2	-0.45	-0.48	-0.51	-0.55	-0.58	-0.62	-0.66	-0.71
Catalyst-H_2O	-0.23	-0.25	-0.27	-0.28	-0.30	-0.32	-0.35	-0.37
Catalyst-H*	-0.20	-0.22	-0.23	-0.25	-0.27	-0.28	-0.30	-0.32

$\Delta E_{adsorption}$ in water

Catalysts	Co-Si_{48}	Co-Si_{60}	Co-SiNT (5, 0)	Co-SiNT (6, 0)	Fe-Si_{48}	Fe-Si_{60}	Fe-SiNT (5, 0)	Fe-SiNT (6, 0)
Catalyst-*OH	-4.02	-4.29	-4.58	-4.88	-5.21	-5.56	-5.93	-6.33
Catalyst-*O	-4.37	-4.66	-4.97	-5.31	-5.66	-6.04	-6.45	-6.88
Catalyst-*OOH	-2.13	-2.27	-2.43	-2.59	-2.76	-2.95	-3.14	-3.35
Catalyst-O_2	-0.55	-0.59	-0.63	-0.67	-0.72	-0.77	-0.82	-0.87
Catalyst-H_2O	-0.29	-0.31	-0.33	-0.35	-0.37	-0.40	-0.43	-0.45
Catalyst-H*	-0.25	-0.27	-0.29	-0.31	-0.33	-0.35	-0.37	-0.40

The *O has the most negative $\Delta E_{adsorption}$ than *OH, *OOH, *H, O_2 and H_2O species on Co-Si_{48}, Co-Si_{60}, Co-SiNT (5, 0), Co-SiNT (6, 0), Fe-Si_{48}, Fe-Si_{60}, Fe-SiNT (5, 0), Fe-SiNT (6, 0) in gas phase and water. The *H and H_2O species have the lowest $\Delta E_{adsorption}$ than *OH, *OOH, *O and O_2 species on Co-Si_{48}, Co-Si_{60}, Co-SiNT (5, 0), Co-SiNT (6, 0), Fe-Si_{48}, Fe-Si_{60}, Fe-SiNT (5, 0), Fe-SiNT (6, 0) in gas phase and water. The H_2O is adsorbed on Co-Si_{48}, Co-Si_{60}, Co-SiNT (5, 0), Co-SiNT (6, 0), Fe-Si_{48}, Fe-Si_{60}, Fe-SiNT (5, 0), Fe-SiNT (6, 0) with low $\Delta E_{adsorption}$ in gas phase and water, so it can be desorbed from surfaces of catalysts with low energy. The H_2O desorption is final step of ORR and OER processes and Co-Si_{48}, Co-Si_{60}, Co-SiNT (5, 0), Co-SiNT (6, 0), Fe-Si_{48}, Fe-Si_{60}, Fe-SiNT (5, 0), Fe-SiNT (6, 0) have acceptable potential to desorb the H_2O in normal temperature.

The calculated orbital energy of and charge (q) values of complexes of metal doped Si-nanostructures with species are presented in Table 2. The E_{HLG} values of complexes of *OH with Co-Si_{48}, Co-Si_{60}, Co-SiNT (5, 0), Co-SiNT (6, 0), Fe-Si_{48}, Fe-Si_{60}, Fe-SiNT (5, 0), Fe-SiNT (6, 0) are 3.771, 3.403, 3.046, 2.692, 2.362, 2.033, 1.714 and 1.404 eV, respectively. The E_{HLG} values of complexes of H_2O with Co-Si_{48}, Co-Si_{60}, Co-SiNT (5, 0), Co-SiNT (6, 0), Fe-Si_{48}, Fe-Si_{60}, Fe-SiNT (5, 0), Fe-SiNT (6, 0) are 3.032, 2.736, 2.449, 2.169, 1.899, 1.636, 1.378 and 1.128 eV, respectively. The E_{HLG} values of complexes of O_2 with Co-Si_{48}, Co-Si_{60}, Co-SiNT (5, 0), Co-SiNT (6, 0), Fe-Si_{48}, Fe-Si_{60}, Fe-SiNT (5, 0), Fe-SiNT (6, 0) are 3.372, 3.043, 2.723, 2.413, 2.111, 1.819, 1.533 and 1.255 eV, respectively.

The q values of complexes of *OOH with Co-Si_{48}, Co-Si_{60}, Co-SiNT (5, 0), Co-SiNT (6, 0), Fe-Si_{48}, Fe-Si_{60}, Fe-SiNT (5, 0), Fe-SiNT (6, 0) are 0.816, 0.828, 0.840, 0.852, 0.865, 0.877, 0.890 and 0.816 *e*, respectively. The q values of complexes of *O with Co-Si_{48}, Co-Si_{60}, Co-SiNT (5, 0), Co-SiNT (6, 0), Fe-Si_{48}, Fe-Si_{60}, Fe-SiNT (5, 0), Fe-SiNT (6, 0) are 0.891, 0.904, 0.917, 0.930, 0.944, 0.957, 0.971 and 0.891 *e*, respectively. The q values of complexes of *H on Co-Si_{48}, Co-Si_{60}, Co-SiNT (5, 0), Co-SiNT (6, 0), Fe-Si_{48}, Fe-Si_{60}, Fe-SiNT (5, 0), Fe-SiNT (6, 0) are 0.315, 0.319, 0.324, 0.329, 0.333, 0.338, 0.343 and 0.315 *e*, respectively.

Table 2 The E_{HOMO}, E_{LUMO} and E_{HLG} in eV and charge (q) in *e* of metal doped Si-nanostructures and their complexes with species

Catalysts	E_{HOMO}		E_{LUMO}		E_{HLG}		Charge (q)	
Co-Si_{48}	-5.22		-3.18		2.04		0.912	
Co-Si_{60}	-5.11		-3.25		1.86		0.925	
Co-SiNT(5, 0)	-5.01		-3.33		1.68		0.938	
Co-SiNT(6, 0)	-4.92		-3.41		1.49		0.952	
Fe-Si_{48}	-4.81		-3.49		1.31		0.966	
Fe-Si_{60}	-4.70		-3.57		1.13		0.978	
Fe-SiNT(5, 0)	-4.61		-3.67		0.93		0.990	
Fe-SiNT(6, 0)	-4.51		-3.75		0.76		0.998	
E_{HOMO} in eV								
Catalysts	Co-Si_{48}	Co-Si_{60}	Co-SiNT (5, 0)	Co-SiNT (6, 0)	Fe-Si_{48}	Fe-Si_{60}	Fe-SiNT (5, 0)	Fe-SiNT (6, 0)
Catalyst-*OH	-6.779	-6.484	-6.203	-5.933	-5.676	-5.428	-5.193	-4.967
Catalyst-*O	-6.716	-6.424	-6.145	-5.878	-5.622	-5.377	-5.144	-4.920
Catalyst-*OOH	-6.154	-5.887	-5.630	-5.385	-5.152	-4.927	-4.714	-4.509
Catalyst-O_2	-6.063	-5.800	-5.548	-5.307	-5.076	-4.856	-4.645	-4.443
Catalyst-H_2O	-5.450	-5.213	-4.987	-4.770	-4.563	-4.365	-4.174	-3.993
Catalyst-H*	-5.211	-4.985	-4.768	-4.561	-4.362	-4.173	-3.992	-3.818
E_{LUMO} in eV								
Catalysts	Co-Si_{48}	Co-Si_{60}	Co-SiNT (5, 0)	Co-SiNT (6, 0)	Fe-Si_{48}	Fe-Si_{60}	Fe-SiNT (5, 0)	Fe-SiNT (6, 0)
Catalyst-*OH	-3.008	-3.145	-3.288	-3.437	-3.593	-3.757	-3.928	-4.106
Catalyst-*O	-2.98	-3.115	-3.257	-3.405	-3.56	-3.722	-3.891	-4.068
Catalyst-*OOH	-2.731	-2.855	-2.985	-3.12	-3.262	-3.41	-3.565	-3.727
Catalyst-O_2	-2.691	-2.813	-2.941	-3.074	-3.214	-3.36	-3.513	-3.673
Catalyst-H_2O	-2.418	-2.528	-2.643	-2.763	-2.889	-3.02	-3.158	-3.301
Catalyst-H*	-2.312	-2.417	-2.527	-2.642	-2.762	-2.888	-3.019	-3.156
E_{HLG} in eV								
Catalysts	Co-Si_{48}	Co-Si_{60}	Co-SiNT (5, 0)	Co-SiNT (6, 0)	Fe-Si_{48}	Fe-Si_{60}	Fe-SiNT (5, 0)	Fe-SiNT (6, 0)
Catalyst-*OH	3.771	3.403	3.046	2.699	2.362	2.033	1.714	1.404
Catalyst-*O	3.736	3.371	3.017	2.673	2.339	2.014	1.698	1.390
Catalyst-*OOH	3.423	3.089	2.764	2.449	2.143	1.845	1.556	1.274
Catalyst-O_2	3.372	3.043	2.723	2.413	2.111	1.819	1.533	1.255
Catalyst-H_2O	3.032	2.736	2.449	2.169	1.899	1.636	1.378	1.128
Catalyst-H*	2.899	2.616	2.342	2.075	1.815	1.564	1.318	1.079
Charge (q) in e								
Catalysts	Co-Si_{48}	Co-Si_{60}	Co-SiNT (5, 0)	Co-SiNT (6, 0)	Fe-Si_{48}	Fe-Si_{60}	Fe-SiNT (5, 0)	Fe-SiNT (6, 0)
Catalyst-*OH	0.899	0.912	0.926	0.939	0.953	0.966	0.980	0.899
Catalyst-*O	0.891	0.904	0.917	0.930	0.944	0.957	0.971	0.891
Catalyst-*OOH	0.816	0.828	0.840	0.852	0.865	0.877	0.890	0.816
Catalyst-O_2	0.503	0.511	0.518	0.526	0.533	0.541	0.549	0.503
Catalyst-H_2O	0.421	0.427	0.433	0.440	0.446	0.452	0.459	0.421
Catalyst-H*	0.315	0.319	0.324	0.329	0.333	0.338	0.343	0.315

The *O has the lowest E_{HLG} values and the highest q values than *OH, *OOH, *H, O_2 and H_2O species on Co-Si_{48}, Co-Si_{60}, Co-SiNT (5, 0), Co-SiNT (6, 0), Fe-Si_{48}, Fe-Si_{60}, Fe-SiNT (5, 0), Fe-SiNT (6, 0). The *H and H_2O species have the highest E_{HLG} values and the lowest q

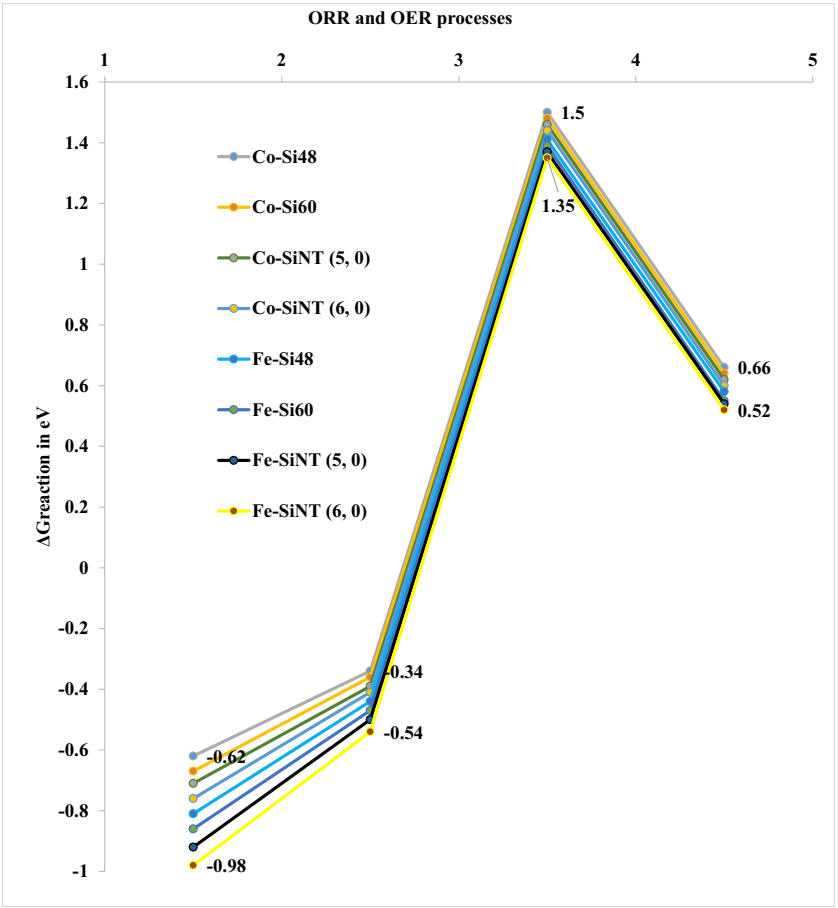

Fig. 2 The chart of $\Delta G_{reaction}$ on metal doped Si-nanostructures

values than *OH, *OOH, *O and O_2 species on Co and Fe doped Si-nanotubes and Co and Fe doped Si-nanocages.

3.3 ORR and OER Mechanisms on Metal Doped Si-Nanostructures

In the ORR and OER processes as the first step the O_2 molecules are adsorbed on Co-Si_{48}, Co-Si_{60}, Co-SiNT (5, 0), Co-SiNT (6, 0), Fe-Si_{48}, Fe-Si_{60}, Fe-SiNT (5, 0), Fe-SiNT (6, 0). In the next step for ORR and OER processes the adsorbed O_2 molecules are joined to *H and then the *OOH is created on surfaces of Co-Si_{48}, Co-Si_{60}, Co-SiNT (5, 0), Co-SiNT (6, 0), Fe-Si_{48}, Fe-Si_{60}, Fe-SiNT (5, 0), Fe-SiNT (6, 0). The adsorption of O_2 molecules and the creation of *OOH on surfaces of Co-Si_{48}, Co-Si_{60}, Co-SiNT (5, 0), Co-SiNT (6, 0), Fe-Si_{48}, Fe-Si_{60}, Fe-SiNT (5, 0), Fe-SiNT (6, 0) have low activation barrier energy in normal temperature. It can be concluded that the formation of *OOH on surfaces of Co-Si_{48}, Co-Si_{60}, Co-SiNT (5, 0), Co-SiNT (6, 0), Fe-Si_{48}, Fe-Si_{60}, Fe-SiNT (5, 0), Fe-SiNT (6, 0) can be considered as the first step for ORR and OER processes.

The overall reaction steps for ORR and OER processes through 4 electron reaction steps on surfaces of Co-Si_{48}, Co-Si_{60}, Co-SiNT (5, 0), Co-SiNT (6, 0), Fe-Si_{48}, Fe-Si_{60}, Fe-SiNT (5, 0), Fe-SiNT (6, 0) can be calculated via Eqs. 9, 10, 11 and 12 as following [60–62]:

step 1) $OH^- + \text{Si-nanostructure} \rightarrow \text{Si-nanostructure-*OH} + e.^-$ (9)

step 2) $OH^- + \text{Si-nanostructure -*OH} \rightarrow \text{Si-nanostructure -*O} + H_2O + e.^-$ (10)

step 3) $OH^- + \text{Si-nanostructure -*O} \rightarrow \text{Si-nanostructure -*OOH} + e.^-$ (11)

step 4) $OH^- + \text{Si-nanostructure -*OOH} \rightarrow \text{surface*} + O_2 + H_2O + e.^-$ (12)

The calculated $\Delta G_{reaction}$ of these reaction steps ($OH^- + \text{Si-nanostructure} \rightarrow \text{Si-nanostructure-*OH} + e^- \rightarrow \text{Si-nanostructure -*O} + H_2O + e^- \rightarrow \text{Si-nanostructure -*OOH} + e^- \rightarrow \text{surface*} + O_2 + H_2O + e^-$) on surfaces of Co-$Si_{48}$, Co-$Si_{60}$, Co-SiNT (5, 0), Co-SiNT (6, 0), Fe-Si_{48}, Fe-Si_{60}, Fe-SiNT (5, 0), Fe-SiNT (6, 0) in gas phase and water are presented in Table 3. The calculated overpotential of OER and ORR (η_{OER} and η_{ORR}) processes on surfaces of Co-Si_{48}, Co-Si_{60}, Co-SiNT (5, 0), Co-SiNT (6, 0), Fe-Si_{48}, Fe-Si_{60}, Fe-SiNT (5, 0), Fe-SiNT (6, 0) in gas phase and water are reported in Table 3. The chart of $\Delta G_{reaction}$ of ORR and OER processes on surfaces of Co-Si_{48}, Co-Si_{60},

Table 3 The $\Delta G_{reaction}$ in eV of reaction steps on metal doped Si-nanostructures at T = 298 K in gas phase and water and overpotential in V on metal doped Si-nanostructures in gas phase and water

$\Delta G_{reaction}$ in gas phase								
Catalysts	Co-Si_{48}	Co-Si_{60}	Co-SiNT (5, 0)	Co-SiNT (6, 0)	Fe-Si_{48}	Fe-Si_{60}	Fe-SiNT (5, 0)	Fe-SiNT (6, 0)
$OH^- \rightarrow *OH$	-0.62	-0.67	-0.71	-0.76	-0.81	-0.86	-0.92	-0.98
$OH^- + *OH \rightarrow *O + H_2O$	-0.34	-0.36	-0.39	-0.41	-0.44	-0.47	-0.50	-0.54
$OH^- + *O \rightarrow *OOH$	1.50	1.48	1.46	1.44	1.41	1.39	1.37	1.35
$OH^- + *OOH \rightarrow O_2 + H_2O$	0.66	0.64	0.62	0.60	0.58	0.55	0.54	0.52
$\Delta G_{reaction}$ in water								
Catalysts	Co-Si_{48}	Co-Si_{60}	Co-SiNT (5, 0)	Co-SiNT (6, 0)	Fe-Si_{48}	Fe-Si_{60}	Fe-SiNT (5, 0)	Fe-SiNT (6, 0)
$OH^- \rightarrow *OH$	-0.77	-0.82	-0.88	-0.94	-1.00	-1.07	-1.14	-1.21
$OH^- + *OH \rightarrow *O + H_2O$	-0.42	-0.45	-0.48	-0.51	-0.55	-0.58	-0.62	-0.66
$OH^- + *O \rightarrow *OOH$	1.22	1.20	1.18	1.16	1.15	1.13	1.11	1.09
$OH^- + *OOH \rightarrow O_2 + H_2O$	0.54	0.52	0.50	0.48	0.47	0.45	0.43	0.42
Catalysts	η_{OER} in gas phase		η_{ORR} in gas phase		Catalysts		η_{OER} in water	η_{ORR} in water
Co-Si_{48}	1.54		1.37		Co-Si_{48}		1.38	1.24
Co-Si_{60}	1.48		1.32		Co-Si_{60}		1.33	1.20
Co-SiNT(5, 0)	1.43		1.28		Co-SiNT(5, 0)		1.28	1.15
Co-SiNT(6, 0)	1.38		1.23		Co-SiNT(6, 0)		1.24	1.11
Fe-Si_{48}	1.32		1.19		Fe-Si_{48}		1.19	1.07
Fe-Si_{60}	1.28		1.15		Fe-Si_{60}		1.15	1.04
Fe-SiNT(5, 0)	1.23		1.11		Fe-SiNT(5, 0)		1.10	1.00
Fe-SiNT(6, 0)	1.18		1.07		Fe-SiNT(6, 0)		1.06	0.97

Co-SiNT (5, 0), Co-SiNT (6, 0), Fe-Si_{48}, Fe-Si_{60}, Fe-SiNT (5, 0), Fe-SiNT (6, 0) are presented in Fig. 2.

In the step 1 ($OH^- + $Si-nanostructure $\rightarrow$ Si-nanostructure-$*OH + e^-$) the OH is adsorbed on surface of Co-Si_{48}, Co-Si_{60}, Co-SiNT (5, 0), Co-SiNT (6, 0), Fe-Si_{48}, Fe-Si_{60}, Fe-SiNT (5, 0), Fe-SiNT (6, 0). The $\Delta G_{reaction}$ values of this step on Co-Si_{48}, Co-Si_{60}, Co-SiNT (5, 0), Co-SiNT (6, 0), Fe-Si_{48}, Fe-Si_{60}, Fe-SiNT (5, 0), Fe-SiNT (6, 0) in gas phase are -0.62, -0.67, -0.71, -0.76, -0.81, -0.86, -0.92 and -0.98 eV. The $\Delta G_{reaction}$ values of this step on Co-Si_{48}, Co-Si_{60}, Co-SiNT (5, 0), Co-SiNT (6, 0), Fe-Si_{48}, Fe-Si_{60}, Fe-SiNT (5, 0), Fe-SiNT (6, 0) in water are -0.77, -0.82, -0.88, -0.94, -1.00, -1.07, -1.14 and -1.21 eV, respectively.

In the step 2 ($OH^- + $Si-nanostructure -$*OH \rightarrow$ Si-nanostructure -$*O + H_2O + e^-$) the *OH on surfaces of Co-Si_{48}, Co-Si_{60}, Co-SiNT (5, 0), Co-SiNT (6, 0), Fe-Si_{48}, Fe-Si_{60}, Fe-SiNT (5, 0), Fe-SiNT (6, 0) is adsorbed the other OH^-. The H_2O molecule is released from surfaces of Co-Si_{48}, Co-Si_{60}, Co-SiNT (5, 0), Co-SiNT (6, 0), Fe-Si_{48}, Fe-Si_{60}, Fe-SiNT (5, 0), Fe-SiNT (6, 0) and the Si-nanostructure -*O is created [63–65]. The $\Delta G_{reaction}$ values of this step on Co-Si_{48}, Co-Si_{60}, Co-SiNT (5, 0), Co-SiNT (6, 0), Fe-Si_{48}, Fe-Si_{60}, Fe-SiNT (5, 0), Fe-SiNT (6, 0) in gas phase are -0.34, -0.36, -0.39, -0.41, -0.44, -0.47, -0.50 and -0.54 eV. The $\Delta G_{reaction}$ values of this step on Co-Si_{48}, Co-Si_{60}, Co-SiNT (5, 0), Co-SiNT (6, 0), Fe-Si_{48}, Fe-Si_{60}, Fe-SiNT (5, 0), Fe-SiNT (6, 0) in water are -0.42, -0.45, -0.48, -0.51, -0.55, -0.58, -0.62 and -0.66 eV, respectively.

In step 3 ($OH^- + $Si-nanostructure -$*O \rightarrow$ Si-nanostructure -$*OOH + e^-$) the Si-nanostructure -*O is adsorbed the other OH^- on surfaces of Co-Si_{48}, Co-Si_{60}, Co-SiNT (5, 0), Co-SiNT (6, 0), Fe-Si_{48}, Fe-Si_{60}, Fe-SiNT (5, 0), Fe-SiNT (6, 0) and the Si-nanostructure -*OOH is created. The $\Delta G_{reaction}$ values of this step on Co-Si_{48}, Co-Si_{60}, Co-SiNT (5, 0), Co-SiNT (6, 0), Fe-Si_{48}, Fe-Si_{60}, Fe-SiNT (5, 0), Fe-SiNT (6, 0) in gas phase are 1.50, 1.48, 1.46, 1.44, 1.41, 1.39, 1.37 and 1.35 eV. The $\Delta G_{reaction}$ values of this step on Co-Si_{48}, Co-Si_{60}, Co-SiNT (5, 0), Co-SiNT (6, 0), Fe-Si_{48}, Fe-Si_{60}, Fe-SiNT (5, 0), Fe-SiNT (6, 0) in water are 1.22, 1.20, 1.18, 1.16, 1.15, 1.13, 1.11 and 1.09 eV, respectively.

In step 4 ($OH^- + $Si-nanostructure -$*OOH \rightarrow$ surface$* + O_2 + H_2O + e^-$) the Si-nanostructure -*OOH is adsorbed the other OH^- and the second H_2O molecule is released from surfaces of Co-Si_{48}, Co-Si_{60}, Co-SiNT (5, 0), Co-SiNT (6, 0), Fe-Si_{48}, Fe-Si_{60}, Fe-SiNT (5, 0), Fe-SiNT (6, 0). The $\Delta G_{reaction}$ values of this step on Co-Si_{48}, Co-Si_{60}, Co-SiNT (5, 0), Co-SiNT (6, 0), Fe-Si_{48}, Fe-Si_{60}, Fe-SiNT (5, 0), Fe-SiNT (6, 0) in gas phase are 0.66, 0.64, 0.62, 0.60, 0.58, 0.55, 0.54 and 0.52 eV, respectively. The $\Delta G_{reaction}$ values of this step on Co-Si_{48}, Co-Si_{60}, Co-SiNT

(5, 0), Co-SiNT (6, 0), Fe-Si_{48}, Fe-Si_{60}, Fe-SiNT (5, 0), Fe-SiNT (6, 0) in water are 0.54, 0.52, 0.50, 0.48, 0.47, 0.45, 0.43 and 0.42 eV.

The overpotential of OER processes on Co-Si_{48}, Co-Si_{60}, Co-SiNT (5, 0), Co-SiNT (6, 0), Fe-Si_{48}, Fe-Si_{60}, Fe-SiNT (5, 0), Fe-SiNT (6, 0) in gas phase are 1.54, 1.48, 1.43, 1.38, 1.32, 1.28, 1.23 and 1.18 eV, respectively. The overpotential of ORR processes on Co-Si_{48}, Co-Si_{60}, Co-SiNT (5, 0), Co-SiNT (6, 0), Fe-Si_{48}, Fe-Si_{60}, Fe-SiNT (5, 0), Fe-SiNT (6, 0) in gas phase are 1.38, 1.33, 1.28, 1.24, 1.19, 1.15, 1.10 and 1.06 eV.

Results indicated that the reactions step for OOH* creation for OER processes is the potential-determining step on Co-Si_{48}, Co-Si_{60}, Co-SiNT (5, 0), Co-SiNT (6, 0), Fe-Si_{48}, Fe-Si_{60}, Fe-SiNT (5, 0), Fe-SiNT (6, 0) [66]. The potential-determining step for ORR processes is the step of OH* elimination from surfaces of Co-Si_{48}, Co-Si_{60}, Co-SiNT (5, 0), Co-SiNT (6, 0), Fe-Si_{48}, Fe-Si_{60}, Fe-SiNT (5, 0), Fe-SiNT (6, 0).

The overpotential of OER processes on Co-Si_{48}, Co-Si_{60}, Co-SiNT (5, 0), Co-SiNT (6, 0), Fe-Si_{48}, Fe-Si_{60}, Fe-SiNT (5, 0), Fe-SiNT (6, 0) in water are 1.37, 1.32, 1.28, 1.23, 1.19, 1.15, 1.11 and 1.07 eV, respectively. The overpotential of ORR processes on Co-Si_{48}, Co-Si_{60}, Co-SiNT (5, 0), Co-SiNT (6, 0), Fe-Si_{48}, Fe-Si_{60}, Fe-SiNT (5, 0), Fe-SiNT (6, 0) in water are 1.24, 1.20, 1.15, 1.11, 1.07, 1.04, 1.00 and 0.97 eV, respectively.

The $\Delta G_{reaction}$ values of reaction steps 1 and 2 of ORR and OER processes on Co-Si_{48}, Co-Si_{60}, Co-SiNT (5, 0), Co-SiNT (6, 0), Fe-Si_{48}, Fe-Si_{60}, Fe-SiNT (5, 0), Fe-SiNT (6, 0) are negative values. The Fe doped Si-nanotubes and Si-nanocages for reaction steps of ORR and OER processes have more negative the $\Delta G_{reaction}$ values than Co doped Si-nanotubes and Si-nanocages. The Co and Fe doped Si-nanotubes for reaction steps of ORR and OER processes have more negative $\Delta G_{reaction}$ values than Co and Fe doped Si-nanocages. Finally, the Co and Fe doped Si-nanotubes and Si-nanocages (Co-Si_{48}, Co-Si_{60}, Co-SiNT (5, 0), Co-SiNT (6, 0), Fe-Si_{48}, Fe-Si_{60}, Fe-SiNT (5, 0), Fe-SiNT (6, 0)) have acceptable potential to catalyze the OER and ORR processes.

4 Conclusion

The potential of Co-Si_{48}, Co-Si_{60}, Co-SiNT (5, 0), Co-SiNT (6, 0), Fe-Si_{48}, Fe-Si_{60}, Fe-SiNT (5, 0), Fe-SiNT (6, 0) to catalyze the ORR and OER are investigated in gas phase and water. Tthe $E_{formation}$ of Co-Si_{48}, Co-Si_{60}, Fe-Si_{48} and Fe-Si_{60} are -4.15, -4.25, -4.56 and -4.67 eV, respectively. The $E_{adoption}$ of Co-SiNT (5, 0), Co-SiNT (6, 0), Fe-SiNT (5, 0) and Fe-SiNT (6, 0) are -3.86, -4.03, -4.58 and -4.78 eV, respectively. The Fe doped Si-nanotubes and Si-nanocages have lower E_{HLG} values and higher q values than Co doped Si-nanotubes and Si-nanocages. The H_2O is adsorbed on Si-nanostructures with low $\Delta E_{adsorption}$, so it can be desorbed from surfaces of catalysts with low energy. The reaction steps of ORR on Si-nanostructures are $OH^- +$ Si-nanostructure $\rightarrow$ Si-nanostructure-*OH $+ e^- \rightarrow$ Si-nanostructure -*O $+ H_2O + e^- \rightarrow$ Si-nanostructure -*OOH $+ e^- \rightarrow$ surface* $+ O_2 + H_2O + e^-$. In the step 1 the $\Delta G_{reaction}$ on Co-Si_{48}, Co-Si_{60}, Co-SiNT (5, 0) and Co-SiNT (6, 0) are -0.62, -0.67, -0.71 and -0.76 eV. The $\Delta G_{reaction}$ of step 2 on Fe-Si_{48}, Fe-Si_{60}, Fe-SiNT (5, 0) and Fe-SiNT (6, 0) are -0.44, -0.47, -0.50 and -0.54 eV, respectively. Results indicated that the reactions step of OOH* creation for OER and OH* elimination for ORR are the potential-determining steps. The overpotential of OER processes on Co-Si_{48}, Co-Si_{60}, Co-SiNT (5, 0), Co-SiNT (6, 0), Fe-Si_{48}, Fe-Si_{60}, Fe-SiNT (5, 0), Fe-SiNT (6, 0) in gas phase are 1.54, 1.48, 1.43, 1.38, 1.32, 1.28, 1.23 and 1.18 eV. Finally, the Co and Fe doped Si-nanotubes and Si-nanocages (Co-Si_{48}, Co-Si_{60}, Co-SiNT (5, 0), Co-SiNT (6, 0), Fe-Si_{48}, Fe-Si_{60}, Fe-SiNT (5, 0), Fe-SiNT (6, 0)) have acceptable potential to catalyze the OER and ORR processes.

Supplementary Information The online version contains supplementary material available at https://doi.org/10.1007/s12633-024-02915-y.

Acknowledgements We thank for or university for their helps.

Authors' Contributions Diana Katherine Campoverde Santos: Conceptualization, Methodology, Software, Mohammed Ahmed Mustafa: Formal analysis, Investigation Resources, Pooja Bansal: Validation, Validation, Formal analysis, Harpreet Kaur: Software, Validation, Writing—Original Draft, Mahamedha Deorari: Writing—Review & Editing, Visualization. Data Curation, Farag M. A. Altalbawy: Validation, Formal analysis, Investigation Resources, Dheyaa Yahaia Alhameedi: Validation, Validation, Formal analysis, Mahmood Hasen shuhata Alubiady: Writing—Original Draft, Writing—Review & Editing, Ahmed Muzahem Al-Ani: Conceptualization, Methodology, Software, Visualization, Sally Salih Jumaa: Validation, Formal analysis, Investigation Resources, Munther Kadhim Abosaoda: Software, Validation, Writing—Original Draft, Li Zhang: Formal analysis, Investigation Resources, Validation.

Funding Not applicable.

Availability of Data and Material Not applicable.

Code Availability Not applicable.

Declarations

Consent to Participate I confirmed.

Consent for Publication I confirmed.

Ethical Approval All procedures performed in studies involving human participants were in accordance with the ethical standards of the institutional and/or national research committee and with the 1964 Helsinki declaration and its later amendments or comparable ethical standards.

Competing Interests The authors declare no competing interests.

References

1. Zhang SL, Zhang J, Li Y, Pan Z, Zhang J, Wang W, Xing Z, Cheng W, Cheng H, Tham N, Wang J, Liu Z (2023) ACS Appl Mater Interfaces 15(51):59454–59462
2. Lin F, Li M, Zeng L, Luo M, Guo S (2023) Chem Rev 123(22):12507–12593
3. Qiu Y, Fan J, Wu J, Lu W, Wang S, Wang D, Ge X, Zhao X, Zhang W, Zheng W, Cui X (2023) Nano Lett 23(20):9555–9562
4. Ying J, Xiao Y, Chen J, Hu Z-Y, Tian G, Van Tendeloo G, Zhang Y, Symes MD, Janiak C, Yang X-Y (2023) Nano Lett. 23(16):7371–7378
5. Pal S, Ahmed T, Khatun S, Roy P (2023) ACS Appl Energy Mater 6(15):7737–7784
6. Shen J-F, Hu S-N, Tian N, Li M-Y, Yang S-L, Tian S-Y, Chen M-S, Zhou Z-Y, Sun S-G (2023) ACS Sustain Chem Eng 11(31):11660–11667
7. Wang Z, Tian P, Zhang H, Deng K, Yu H, Xu Y, Li X, Wang H, Wang L (2023) Ino Chem 62(14):5622–5629
8. Young Kim H, Jun M, Lee K, HoonJoo S (2023) ACS Catal. 13(1):355–374
9. Cao F, Zhang H, Duan X, Li X, Ding R, Hua K, Rui Z, Wu Y, Yuan M, Wang J, Li J, Han M, Liu J (2022) ACS Appl Mater Interfaces 14(46):51975–51982
10. Yang L, Hou S, Zhu S, Shi Z, Wang X, Jiang J, Chu Y, Bai J, Wang Y, Zhang L, Jiang Z, Liu C, Xing W, Ge J (2022) ACS Catal 12(21):13523–13532
11. Liu J, Liu S, Yan F, Wen Z, Chen W, Liu X, Liu Q, Shang J, Yu R, Su D, Shui J (2022) J Am Chem Soc 144(41):19106–19114
12. Zhang K, He Y, Guo R, Wang W, Zhan Q, Li R, He T, Wu C, Jin M (2022) ACS Energy Lett 7(10):3329–3336
13. Xie M, Zhang B, Jin Z, Li P, Yu G (2022) ACS Nano 16(9):13715–13727
14. Wang H, Zhou T, Deng K, Tian W, Yu H, Xu Y, Li X, Wang Z, Wang L (2022) Energy Fuels 36(14):7775–7781
15. Hu J, Fang C, Jiang X, Zhang D, Cui Z (2022) Inorg Chem 61(24):9352–9363
16. Wu H, Zhong H, Pan Y, Li H, Zeng J (2022) Ind Eng Chem Res 61(22):7504–7512
17. Yu YX (2019) J Phys Chem C 123:205–213
18. Li JH, Wu J, Yu YX (2020) J Phys Chem C 124:9089–9098
19. Li JH, Yu YX (2021) Nanoscale 13:20637–20648
20. Li JH, Wu J, Yu YX (2021) J Mater Chem A 9:10186–10198
21. Li JH, Yu YX (2021) Chemsuschem 14:5488–5498
22. Huang Y, Kong F, Tian H, Pei F, Chen Y, Meng G, Chang Z, Chen C, Cui X, Shi J (2022) ACS Sustain Chem Eng 10(19):6370–6381
23 Campos-Roldán CA, Parnière A, Donzel N, Pailloux F, Blanchard P-Y, Jones DJ, Rozière J, Cavaliere S (2022) ACS Appl Energy Mater 5(3):3319–3328
24. Chen Y, Li W, Yao Y, Gogoi P, Deng X, Xie Y, Yang Z, Wang Y, Li YC (2022) ACS Appl Mater Interfaces 14(10):12257–12263
25 Nair AS, Anoop A, Ahuja R, Pathak B (2022) J Phys Chem A 126(8):1345–1359
26. Wang W, Liu S, Min C, Zeng M, Shi H, Shao R, Liu S, Xu Z, Xia Y, Li N (2022) ACS Appl Energy Mater 5(2):2036–2044
27. Tang Y, Zeng Z, Yi L, Zhu S, Li X, Li H, Lv N, Xu Y, Zhang Q, Wang Y (2022) Energy Fuels 36(4):2068–2074
28 Noh S, Le T-H, Jo H, Kim S, Yoon H (2021) ACS Appl Nano Mater 4(12):14094–14104
29 Lim J, Shin K, Bak J, Han Roh J, Jae Lee S (2021) Chem Mater 33(22):8895–8903
30. Campos-Roldán CA, Pailloux F, Blanchard P-Y, Jones DJ, Rozière J, Cavaliere S (2021) ACS Catal. 11(21):13519–13529
31. Huang L, Zheng X, Gao G, Zhang H, Rong K, Chen J, Liu Y, Zhu X, Wu W, Wang Y, Wang J, Dong S (2021) J Am Chem Soc 143(18):6933–6941
32. Peng B, Liu H, Liu Z, Duan X, Huang Y (2021) J Phys Chem Lett 12(11):2837–2847
33. Wang J, Liu X, Zhao C-X, Song Y-W, Liu J-N, Li X-Y, Bi C-X, Wan X, Shui J, Peng H-J, Li B-Q, Huang J-Q (2024) J Energy Chem 90:511–517
34. Qian Y, Zhang F, Luo X, Zhong Y, Kang DJ, Hu Y (2024) Small 895:1–10
35. Bartók AP, Kondor R, Csányi G (2013) Phys Rev B: Condens Matter Mater Phys 87:184115
36. De S, Bartok AP, Csanyi G, Ceriotti M (2016) Phys Chem Chem Phys 18:13754–13769
37. Zhu L, Amsler M, Fuhrer T, Schäfer B, Faraji S, Rostami S, Ghasemi SA, Sadeghi A, Grauzinyte M, Wolverton C, Goedecker S (2016) J Chem Phys 144:034203
38. Sadeghi A, Ghasemi SA, Schäfer B, Mohr S, Lill MA, Goedecker S (2013) J Chem Phys 139:184118
39. Rupp M, Tkatchenko A, Müller K-R, von Lilienfeld OA (2012) Phys Rev Lett 108:058301
40. Behler J (2015) Int J Quantum Chem 115:1032–1050
41. Gillan MJ, Alfé D, Michaelides A (2016) Perspective: How good is DFT for water. J Chem Phys 144:130901
42. Del Ben M, Schönherr M, Hutter J, VandeVondele J (2013) J Phys Chem Lett 4:3753–3759
43. Del Ben M, Hutter J, VandeVondele J (2015) J Chem Phys 143:054506
44. Verlet L (1967) Phys Rev 159:98–103
45. Elstner M, Porezag D, Jungnickel G, Elsner J, Haugk M, Frauenheim T, Suhai S, Seifert G (1998) Phys Rev B: Condens Matter Mater Phys 58:7260–7268
46. Hu H, Lu Z, Elstner M, Hermans J, Yang W (2007) J Phys Chem A 111:5685–5691
47. Skinner LB, Huang C, Schlesinger D, Pettersson LGM, Nilsson A, Benmore CJ (2013) J Chem Phys 138:074506
48. Hutter J, Iannuzzi M, Schiffmann F, VandeVondele J (2014) Rev: Comput Mol Sci 4:15–25
49. VandeVondele J, Krack M, Mohamed F, Parrinello M, Chassaing T, Hutter J (2005) Comput Phys Commun 167:103–128
50. Lippert G, Hutter J, Parrinello M (1997) Mol Phys 92:477–488
51. Perdew JP, Burke K, Ernzerhof M (1996) Phys Rev Lett 77:3865–3868
52. Yao J, Li C, Sun K, Li H, Li H (2023) IEEE/CVF Int Conf Comput Vis 1:9455–9465
53. Kong Z, Zhang P, Chen J, Zhou H, Ma X, Liang LJ (2021) ACS Omega 6:10936–10943
54. Cui RF, Chen QH, Chen JX (2020) Nanoscale 12:12275–12280
55. Li L, Xu W, Tan Y, Yang J, Tan D (2023) Mech Syst Signal Process 189:110058
56. Li P, Abbas J, Wang Q, Zhang Q, Shah SAR (2024) Gondwana Res 128:86–105
57. Huang J, Cho Y, Zhang Z, Jan A, Kummel AC (2022) ACS Appl Mat Interf 14:15716–15727
58. Cho Y, Huang J, Ahles CF, Zhang Z, Wong K (2022) Appl Sur Sci 600:154010
59. Zhang Z, Passlack M, Pitner G, Kuo CH (2022) ACS Appl Mat Interf 14:11873–11882
60 Jiao Y, Gu L, Jiang Y, Weng M, Yang M (2023) Bioinformatics 39:btac719
61. Jiao Y, Xie N, Gao Y, Wang CC, Sun Y (2022) Euro Conf Comput Vis 1:19–35

62. Jiao Y, Weng M, Yang M (2019) IEEE/CVF Conf Comput Pattern Recog 1:1–10
63. Chen Q, Wang J, Gao M, Liu L, Tao J (2022) Emerg Manag Sci Technol 2:10
64. Qian S, Fang Y, Yao C, Wang Y, Zhang Z et al (2022) Oncol Res 30:53–64
65. Willong L, Gangshin SJ (2023) Synth Chem 2:252–264
66. Kazemi M, Karezani N (2023) Biol Mol Chem 1:15–26